Article

Developmental Cell

Role of Polarized G Protein Signaling in Tracking Pheromone Gradients

Highlights

- Yeast pheromone sensors concentrate at the polarity site during gradient tracking
- The polarity site is mobile, but high pheromone levels restrict its mobility
- G proteins polarize independent of receptor
- Localized pheromone sensing enables tracking of pheromone gradients

Authors

Allison W. McClure, Maria Minakova, Jayme M. Dyer, Trevin R. Zyla, Timothy C. Elston, Daniel J. Lew

Correspondence

timothy_elston@med.unc.edu (T.C.E.), daniel.lew@duke.edu (D.J.L.)

In Brief

Yeast cells find mating partners by polarized growth along a pheromone gradient. This gradient tracking is mediated by a mobile polarity site, whose exploratory wandering slows as pheromone concentration increases. McClure et al. show that pheromone-mediated constraint of wandering requires polarized pheromone sensing machinery to locally influence the polarity site.

McClure et al., 2015, Developmental Cell *35*, 471–482
November 23, 2015
http://dx.doi.org/10.1016/j.devcel.2015.10.024

CellPress

Developmental Cell
Article

Role of Polarized G Protein Signaling in Tracking Pheromone Gradients

Allison W. McClure,[1,4] Maria Minakova,[2,4] Jayme M. Dyer,[1,3,4] Trevin R. Zyla,[1] Timothy C. Elston,[2,*] and Daniel J. Lew[1,*]
[1]Department of Pharmacology and Cancer Biology, Duke University Medical Center, Durham, NC 27710, USA
[2]Department of Pharmacology, University of North Carolina at Chapel Hill, Chapel Hill, NC 27599, USA
[3]Present address: Department of Biology, Massachusetts Institute of Technology, Boston, MA 02139, USA
[4]Co-first author
*Correspondence: timothy_elston@med.unc.edu (T.C.E.), daniel.lew@duke.edu (D.J.L.)
http://dx.doi.org/10.1016/j.devcel.2015.10.024

SUMMARY

Yeast cells track gradients of pheromones to locate mating partners. Intuition suggests that uniform distribution of pheromone receptors over the cell surface would yield optimal gradient sensing. However, yeast cells display polarized receptors. The benefit of such polarization was unknown. During gradient tracking, cell growth is directed by a patch of polarity regulators that wanders around the cortex. Patch movement is sensitive to pheromone dose, with wandering reduced on the up-gradient side of the cell, resulting in net growth in that direction. Mathematical modeling suggests that active receptors and associated G proteins lag behind the polarity patch and act as an effective drag on patch movement. In vivo, the polarity patch is trailed by a G protein-rich domain, and this polarized distribution of G proteins is required to constrain patch wandering. Our findings explain why G protein polarization is beneficial and illuminate a novel mechanism for gradient tracking.

INTRODUCTION

The ability to track chemical gradients underpins a multitude of cell and organismal behaviors. Gradient tracking underlies axon guidance, homing of immune cells toward invaders, chemotaxis of fibroblasts toward wound sites, guidance of sperm toward the egg, and metastasis in cancer (Condeelis et al., 2005; von Philipsborn and Bastmeyer, 2007; Rappel and Loomis, 2009; Raz and Reichman-Fried, 2006; Schnorrer and Dickson, 2004; Swaney et al., 2010). For microorganisms, gradient tracking enhances the search for food or mating partners (Arkowitz, 2009; Sourjik and Wingreen, 2012). Eukaryotic cells are thought to detect small concentration differences across the cell diameter (reviewed in Swaney et al., 2010). Ligands are sensed by G protein-coupled receptors (GPCRs), which signal through heterotrimeric G proteins (reviewed in McCudden et al., 2005). Activated G proteins (Gα-GTP and free Gβγ) then signal through various pathways to the actin cytoskeleton, which controls directional cell growth and migration (McCudden et al., 2005). Despite progress in identifying links between G proteins and the cytoskeleton, we still lack a clear view of how cells can effectively track shallow gradients (Insall, 2013).

The accuracy of spatial gradient sensing is limited by cell size: larger cells can compare ligand concentrations across greater distances. Budding yeast (*Saccharomyces cerevisiae*) are small, yet they can track shallow gradients of peptide pheromones to locate mating partners (Moore et al., 2008; Segall, 1993). Remarkably, yeast pheromone receptors become polarized toward the growing "front" of the cell (Ayscough and Drubin, 1998; Jackson et al., 1991; Moore et al., 2008), thereby reducing the length scale that these tiny cells can use to compare pheromone concentrations. The benefit of polarized receptors presumably outweighs the cost of reduced sensitivity of gradient detection, but the nature of that benefit is unclear. We now suggest that polarized receptor and G protein activity may enable gradient tracking through an unexpected mechanism.

Mating yeast cells come into physical contact by growing a mating projection toward the mating partner (Arkowitz, 2009; Segall, 1993). Directional growth involves targeted delivery and fusion of secretory vesicles (Harold, 1990). Vesicles are delivered by myosin motors along actin "cables," which are bundles of parallel actin filaments nucleated by formins (Moseley and Goode, 2006). Formins are locally recruited to a patch of the cell cortex (the "front" of the cell) by the conserved Rho-family GTPase, Cdc42 (Figure 1A) (Bi and Park, 2012; Chen et al., 2012; Liu et al., 2012). Thus, actin cables are oriented toward Cdc42, and successful gradient tracking requires that the Cdc42 patch be located on the up-gradient side of the cell.

A pheromone gradient is not a prerequisite for polarization: even cells exposed to a uniform pheromone concentration polarize growth (Arkowitz, 2009; Strickfaden and Pryciak, 2008). In these circumstances, the bud-site-selection regulator Rsr1 can bias the polarity axis toward a "default" predetermined landmark (Madden and Snyder, 1992). However, without Rsr1, polarization still occurs at a random location, suggesting that polarity establishment involves an autocatalytic positive feedback loop among the polarity regulators (Dyer et al., 2013; Strickfaden and Pryciak, 2008). When cells are exposed to a pheromone gradient, the gradient overrides the Rsr1 default program to orient the Cdc42 patch (Valtz et al., 1995). In shallow gradients, cells often polarize in the wrong direction, but over time they adjust their Cdc42 patch location to improve alignment with the gradient (Dyer et al., 2013; Moore et al., 2008; Paliwal et al., 2007; Segall, 1993). Such ongoing gradient tracking must overcome the formidable obstacle imposed by

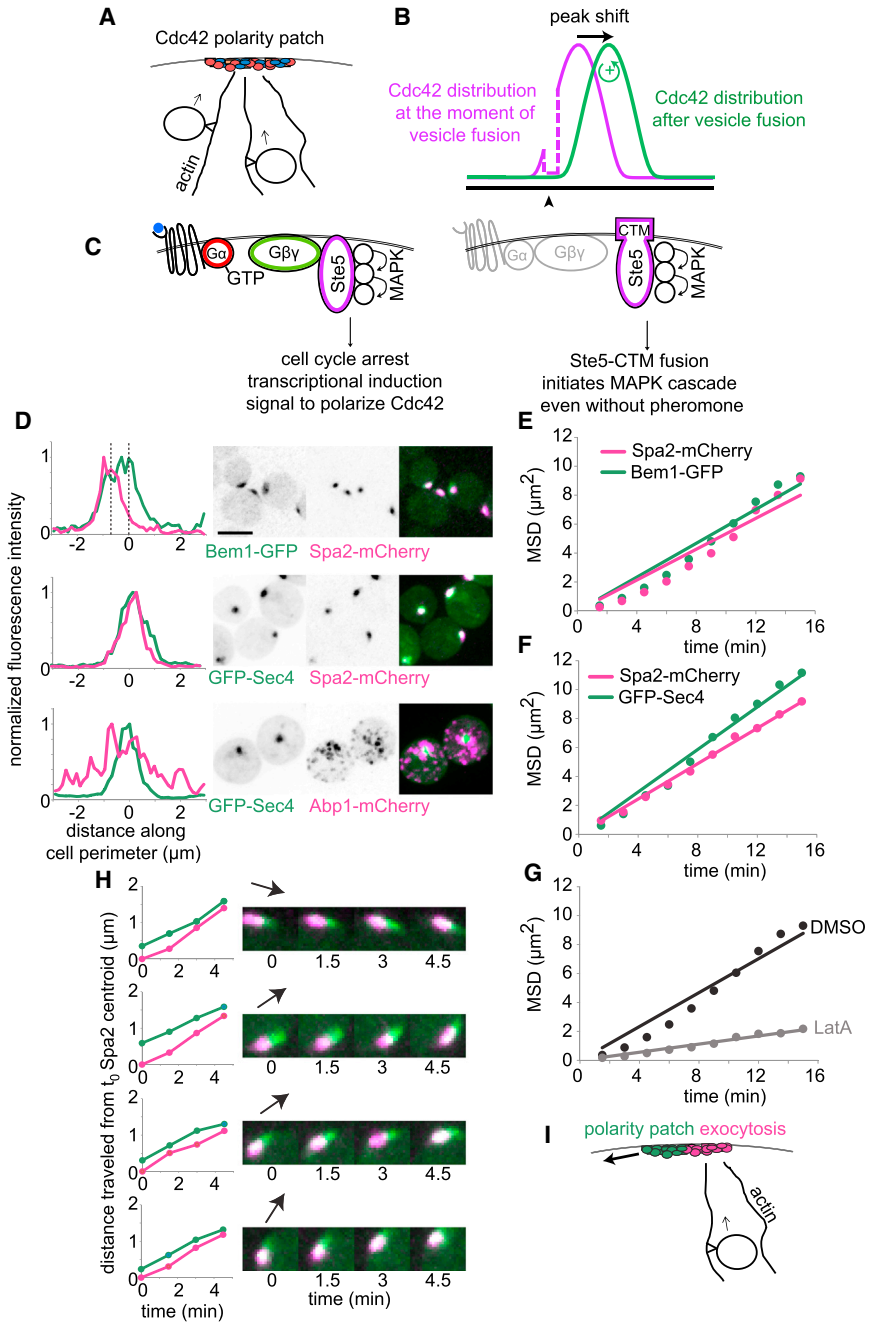

Figure 1. High MAPK Does Not Constrain Wandering

(A) Cdc42 and other polarity proteins cluster at the cell cortex, forming a polarity patch that orients actin cables, which direct myosin-mediated delivery of secretory vesicles to the patch.

(B) Vesicle fusion transiently dilutes polarity factor concentration. When such dilution occurs on one side of the patch, positive feedback preferentially recruits polarity factors to the opposite side, resulting in a displacement of the polarity peak away from the vesicle fusion site (arrowhead).

(C) Left: upon binding pheromone, receptors activate Gα, releasing Gβγ. Free Gβγ recruits Ste5, activating MAPK signaling. Right: Ste5-CTM (Pryciak and Huntress, 1998) is targeted to the plasma membrane even without pheromone.

(D) Cells with the indicated markers (DLY18325, DLY20255, DLY20106) were treated with β-estradiol for 4 hr to induce Ste5-CTM, and imaged. Inverted maximum projections and overlays of representative cells as well as linescans to show the distribution of markers in another cell are shown.

(E) Cells (DLY18325) were treated as in (D). Wandering was detected by time-lapse imaging, and mean-squared displacement (MSD) was calculated ($n > 42$ cells).

(F) Cells (DLY20255) were analyzed as in (E) ($n > 57$ cells).

(G) Cells (DLY18325) were treated as above but loaded on slabs containing DMSO or 200 μM Latruncunlin A (LatA) and imaged 10 min later. MSD was calculated for Bem1-GFP ($n > 40$ cells).

(H) Cells (DLY18325) were treated as in (E), and overlays of Bem1-GFP and Spa2-mCherry (maximum projections) are presented at right. Left: the Bem1-GFP and Spa2-mCherry centroids were used to calculate the distance (in the direction of the motion of the patch along the cell perimeter) from the Spa2-mCherry centroid at $t = 0$.

(I) A wandering polarity patch moves away from exocytosis sites, so the actin-mediated vesicle delivery (Spa2 centroid) trails behind the moving polarity site (Bem1 centroid).

See also Figure S1 and Movie S1.

positive feedback, which reinforces the current location of Cdc42.

Theoretical studies showed that addition of local negative feedback could enable gradient tracking (Meinhardt, 1999). By perturbing the front (the Cdc42 patch), negative feedback could weaken the tendency of the positive-feedback system to continue in the same location, allowing small signal asymmetries to influence the direction of growth. Consistent with the existence of negative feedback, live-cell imaging studies have documented polarity patch "wandering" behavior in yeast cells tracking pheromone gradients (Dyer et al., 2013). Wandering was greatly reduced in cells exposed to the actin depolymerizing drug Latrunculin A, suggesting that F-actin provides a major source of negative feedback. Two mechanisms of negative feedback have been proposed. First, the new membrane added by actin-targeted secretory vesicles could dilute key polarity factors, providing a local perturbation (Figure 1B) (Dyer et al., 2013; Layton et al., 2011; Savage et al., 2012). Consistent with that view, Cdc42 concentration on secretory vesicles is lower than it is at the polarity site (Watson et al., 2014). Second, vesicles may carry negative regulators, such as the Cdc42-directed GAP Bem3, to the polarity site (Knaus et al., 2007; Ozbudak et al., 2005). Stochastic vesicle fusion in the vicinity of the Cdc42 patch can therefore cause the polarity site to gradually "wander" along the cell cortex (Dyer et al., 2013). If pheromone gradients were able to bias such wandering, then that would provide a basis for gradient tracking.

In this study we address the mechanism(s) by which high pheromone concentrations constrain wandering (Dyer et al., 2013). We show that pheromone engages a localized positive feedback loop that stabilizes the polarity patch. This positive feedback requires polarized free Gβγ, and surprisingly, we also found that Gβγ can become polarized independently of GPCR trafficking. Thus, cells polarize both the GPCR and the G protein, reducing the cell surface area in which pheromone concentrations can be sensed. In return, polarized G protein signaling enables a pheromone dose-dependent constraint of polarity patch wandering that can contribute to gradient tracking.

RESULTS

Previous work suggested that at least two pathways constrain wandering of the polarity patch in response to high pheromone levels: one dependent on Rsr1 and another dependent on Far1 (Dyer et al., 2013). The "chemotropism" pathway involving Far1 mediates tracking of the pheromone gradient (Butty et al., 1998; Nern and Arkowitz, 1999; Valtz et al., 1995). As cells lacking Rsr1 appear to mate with high efficiency (Nern and Arkowitz, 1999), the physiological role of the Rsr1 pathway remains unclear. In this study we used *rsr1*Δ mutants in order to focus on constraint of polarity patch wandering by the chemotropism pathway.

Unconstrained Wandering in Cells with High MAPK Activity

Cells responding to pheromone produce free Gβγ that recruits the MAPK scaffold protein Ste5 to the membrane, leading to activation of MAP kinases (Figure 1C) (Hao et al., 2008; Pryciak and Huntress, 1998). We first investigated whether induction of high MAPK activity would suffice to constrain wandering. MAPK activation can be induced downstream of the GPCR/G protein by artificially targeting Ste5 to the plasma membrane with Ste5-CTM (Figure 1C) (Pryciak and Huntress, 1998). Induction of Ste5-CTM led to high levels of MAPK activation and triggered several mating pathway outputs including cell-cycle arrest in G1 and polarization (Figure S1). We imaged several markers to investigate polarity in these cells: Bem1 colocalizes with Cdc42 and mediates positive feedback in polarity establishment (Kozubowski et al., 2008); Spa2 is a formin regulator that helps localize actin cable nucleation (Fujiwara et al., 1998; Pruyne et al., 2004); Sec4 is a secretory vesicle-associated Rab GTPase (Mulholland et al., 1997; Walch-Solimena et al., 1997); and Abp1 is an actin-binding protein that marks endocytosis sites (Kaksonen et al., 2003). Two-color imaging revealed that all of these markers concentrated in the vicinity of the polarity patch (Figure 1D), but Spa2 and Sec4 formed a tighter cluster than Bem1, as previously noted (Lawson et al., 2013). In contrast, Abp1-marked endocytosis sites were clustered in a broader zone surrounding the tight Sec4 patch.

Time-lapse imaging revealed that the polarity patch wandered extensively around the cortex (Movie S1). Wandering was quantified by tracking the patch centroid position and calculating its mean-squared displacement (MSD) (Dyer et al., 2013). Similar MSD profiles were obtained tracking Bem1, Spa2, or Sec4 centroids (Figures 1E and 1F). The high degree of polarity patch wandering in cells expressing Ste5-CTM exceeded that seen in cells tracking pheromone gradients (Dyer et al., 2013). Thus, high-level MAPK activation is not sufficient to constrain wandering.

As in other contexts (Dyer et al., 2013; Ozbudak et al., 2005), wandering in cells expressing Ste5-CTM was greatly reduced upon actin depolymerization (Figure 1G), suggesting that F-actin is responsible for a majority of the wandering. Although Spa2 and Sec4 were tightly co-localized during patch wandering, they were often located off-center with respect to the polarity patch as marked by Bem1 (Figure 1D). Focusing on cases where the polarity patch happened to move consistently in one direction revealed that Spa2 trails behind Bem1 during wandering (Figure 1H). We note that these findings are inconsistent with the hypothesis that vesicles targeted by actin cables provide positive feedback (Freisinger et al., 2013; Slaughter et al., 2009; Smith et al., 2013; Wedlich-Soldner et al., 2003, 2004). If that were the case, the polarity marker should move *toward* (not away from) the actin and vesicle sites, and F-actin should stabilize the location of the patch rather than promoting wandering. On the other hand, our findings are entirely consistent with the idea that off-center actin-mediated vesicle delivery perturbs polarity, either by diluting polarity factors on one side of the patch (Figure 1B) or by delivering negative regulators of polarity (Ozbudak et al., 2005). Thus, when vesicles are delivered to one side of the polarity patch, they drive movement of the patch away from the vesicle delivery site (Figure 1I).

Pheromone Dose-Dependent Constraint of Wandering

When cells expressing Ste5-CTM were exposed to uniform concentrations of pheromone, there was a dose-dependent reduction in polarity site wandering (Figures 2A and 2B), which correlated with a more polarized cell morphology (Figure S2). With no pheromone gradient to bias the direction of polarity patch movement, the degree of wandering could be quantified by calculating an effective diffusion coefficient (D_{patch}, one-fourth the slope of the MSD lines in Figure 2B) (Figure 2C). Thus, pheromone treatment provides dose-dependent constraint of wandering under conditions of high MAPK activity.

To ask how this constraint of wandering might impact the behavior of cells in a pheromone gradient, we used the empirical relation between pheromone concentration and D_{patch} to calculate the probability distribution of patch position for a cell in a pheromone gradient. Consider a circular cell in a linear pheromone gradient (Figure 2D). In terms of the distance s around the cell periphery, the pheromone concentration $c(s)$ is given by

$$c(s) = \alpha_f + \frac{\Delta\alpha_f}{2}\sin\left(\frac{s}{r}\right), \qquad \text{(Equation 1)}$$

where α_f is the pheromone concentration at the center of the cell and $\Delta\alpha_f$ is the difference in concentration between the front and back of the cell. We assume a cell radius of $r = 2.5$ μm and use the relation in Figure 2C to compute $D(s)$ for given values of α_f and $\Delta\alpha_f$. Because locations exposed to higher pheromone have slower wandering, the polarity patch spends more time on the up-gradient side. Movement of the patch is governed by the diffusion equation

$$\frac{\partial}{\partial t}p(s,t) = \frac{\partial^2}{\partial s^2}D(s)p(s,t). \qquad \text{(Equation 2)}$$

The steady-state probability distribution for the position of the patch is given by $p(s) = Z/D(s)$, where Z is the relevant normalization constant. Thus, specific pheromone gradients would lead to

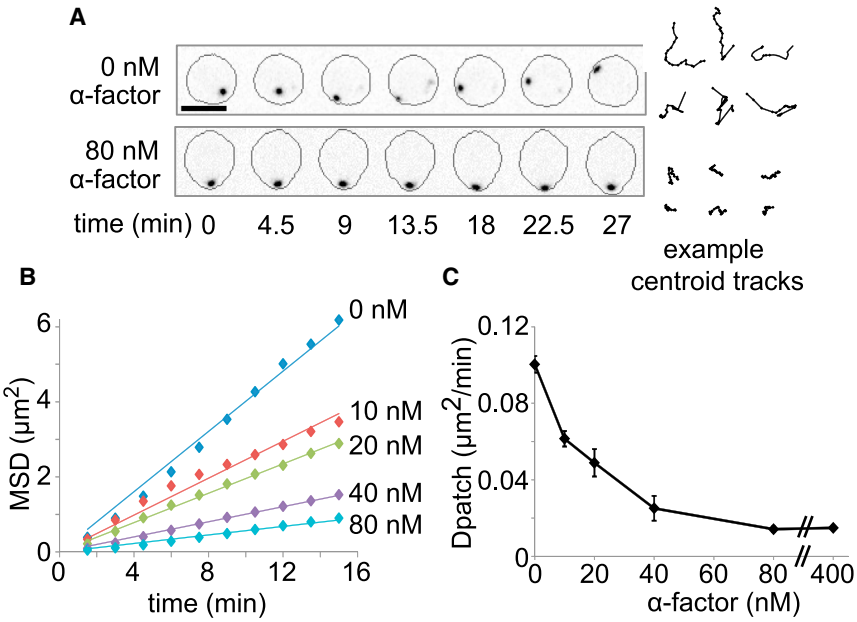

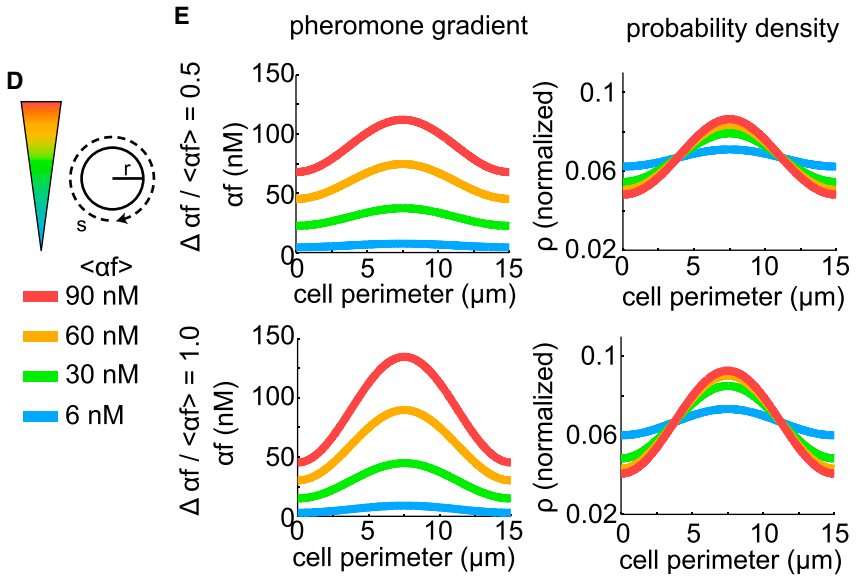

Figure 2. Pheromone Constrains Wandering Independent of MAPK

(A) Cells (DLY18172) were treated with β-estradiol for 4 hr to induce Ste5-CTM, then loaded on a slab with the indicated dose of α-factor (αf) and imaged 20 min later. Right: example of Spa2-mCherry centroid tracks.

(B) Mean-squared displacement (MSD) of the Spa2-mCherry centroid (n > 200 cells) in cells imaged as in (A).

(C) Effective diffusion coefficient of the polarity patch was calculated from the slope of the lines in (B). Mean ± SEM for four independent biological replicates are shown.

(D) Cartoon showing model cell with radius *r* and perimeter *s* in a linear pheromone gradient.

(E) Left: pheromone gradients the model cell was exposed to. All gradients in the same panel have the same ratio of concentration difference to mean concentration (left). Colors indicate different gradients, with mean concentration indicated by color. Right: normalized probability density (ρ) for the polarity patch location in model cells exposed to the same-colored gradients, derived using data in (C). See also Figure S2.

different probability distributions for patch location (Figure 2E). Model performance was poor near the receptor K_D (6 nM) (Jenness et al., 1986) but improved at higher concentrations (while maintaining a constant ratio between gradient steepness and average pheromone concentration), consistent with in vivo findings (Moore et al., 2008; Paliwal et al., 2007; Segall, 1993). Although this toy model is unrealistic in several respects, it suggests that understanding the mechanism by which pheromone concentration constrains patch wandering will provide insight into how yeast cells track gradients.

Constraint of Polarity Patch Wandering Operates via a Gβγ-Far1-Cdc24 Pathway

Previous studies showed that Far1 binds the Cdc42-directed GEF, Cdc24 (Figure 3A); mutations that weaken the Far1-Cdc24 interaction abolish gradient tracking (Nern and Arkowitz, 1998) and allow polarity patch wandering to continue even at high pheromone doses (Figure 3B) (Dyer et al., 2013; Nern and Arkowitz, 2000). Far1 binds free Gβγ, which is thought to target Far1-Cdc24 complexes to sites of G protein activation (Butty et al., 1998; Nern and Arkowitz, 1999). In addition, Far1 cycles in and out of the nucleus, and concentrates a significant fraction of Cdc24 in the nucleus, where it would be unable to activate Cdc42 at the membrane (Blondel et al., 1999; Butty et al., 1998; Nern and Arkowitz, 1999; Shimada et al., 2000). Thus, the Far1-Cdc24 interaction might promote constraint of wandering either by targeting Cdc24 to free Gβγ or by regulating the amount of available Cdc24 in the cytoplasm. We found that in cells expressing Ste5-CTM, the nucleocytoplasmic distribution of Cdc24-GFP was only slightly affected by pheromone treatment (Figure 3C). However, the ability of pheromone to constrain wandering absolutely required *STE4* (encoding Gβ) (Figure 3D). Thus, constraint of wandering operates through a Gβγ-Far1-Cdc24 pathway.

Computational Modeling Suggests that Uniform Recruitment of GEF Would Not Constrain Wandering

To investigate how Gβγ-Far1-Cdc24 could constrain patch wandering, we turned to computational modeling. The model incorporates the positive feedback loop among polarity regulators, Cdc42, Bem1, and Cdc24 (Figure 3E), yielding a polarized patch of Cdc42 (Goryachev and Pokhilko, 2008). It also includes stochastic exocytosis and endocytosis of vesicles, which perturbs

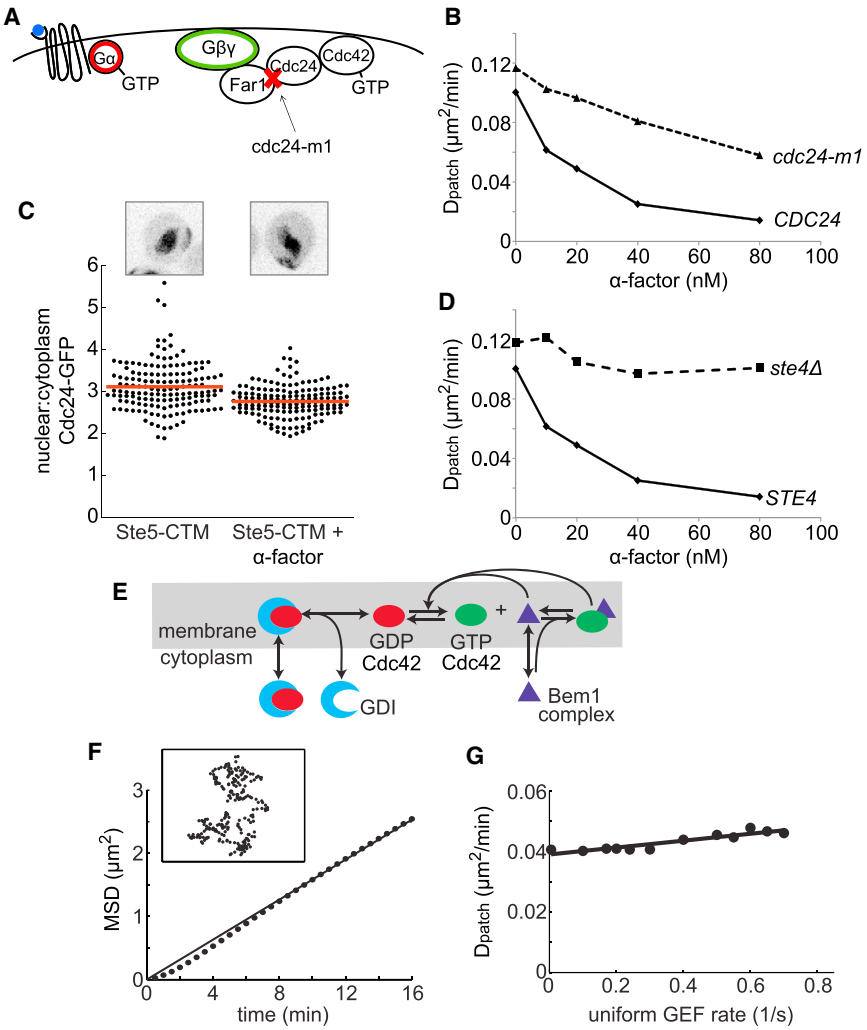

Figure 3. Pheromone Constrains Wandering through GEF Recruitment, but Uniform GEF Recruitment Would Be Insufficient to Constrain Wandering

(A) Free Gβγ recruits a Far1-Cdc24 (GEF) complex to the cortex. *cdc24-m1* reduces Far1-Cdc24 binding.

(B) Cells harboring *cdc24-m1* (DLY18478) were treated and imaged as in Figure 2C, from which the control wild-type data are reproduced (n > 41 cells).

(C) Cells (DLY20226) were treated with β-estradiol for 4 hr, loaded on a slab with 0 nM or 80 nM α-factor, and imaged 20 min later (maximum projections). Graph shows the nuclear:cytoplasm ratio of Cdc24-GFP (each dot is one cell).

(D) Cells lacking Gβ (*ste4Δ*, DLY18425) were imaged and quantified as in (B) (n > 59).

(E) Schematic of model incorporating the protein interactions that mediate positive feedback and Cdc42 clustering. Bem1 complexes containing Cdc24 associate with pre-existing GTP-Cdc42 at the membrane, promoting activation of neighboring GDP-Cdc42. The resulting local depletion of GDP-Cdc42 leads to net delivery of GDP-Cdc42 from the cytoplasm by the GDI, leading to further GTP-Cdc42 accumulation.

(F) MSD from model with vesicle traffic (average of 100 2-hr simulations). Inset: centroid track from one simulation.

(G) The effective patch diffusion coefficients from model with additional uniform cortical GEF were extracted from simulations as in (F) (100 2-hr simulations at each GEF rate).

See also Figure S3 and Movies S2 and S3.

the patch by diluting polarity proteins to yield wandering (Dyer et al., 2013). However, it does not include potential negative regulators of polarity on vesicles. We simulated the time evolution of polarity protein concentrations on the plasma membrane (Movie S2), allowing us to track the centroid of the polarity patch (GTP-Cdc42) (Figure 3F, inset) and calculate the predicted D_{patch} (Figure 3F).

To simulate addition of uniform pheromone, we initially assumed that liberation of free Gβγ all over the cortex would lead to uniform recruitment of Cdc24 to the cortex by Far1. As the level of activity of this uniform GEF was increased, basal levels of GTP-Cdc42 rose, eventually disrupting the ability of the positive feedback loop to maintain polarity (Figure S3). However, as long as the model was able to maintain polarity, additional GEF did not affect wandering (Figure 3G; Movie S3), suggesting that uniformly distributed cortical GEF activity would not be sufficient to constrain wandering.

Computational Modeling Suggests that Polarization of Pheromone-Recruited GEF Could Constrain Wandering

The previous simulations assumed that exposure to uniform pheromone would produce uniformly distributed free Gβγ and hence GEF activity. However, the pheromone receptor, Ste2, becomes polarized in response to uniform pheromone (Ayscough and Drubin, 1998). Pheromone binding triggers endocytosis and degradation of Ste2, accompanied by delivery of newly synthesized Ste2 to the polarity site on secretory vesicles (Hicke and Riezman, 1996; Hicke et al., 1998; Jenness and Spatrick, 1986; Schandel and Jenness, 1994). As diffusion of proteins in the yeast plasma membrane is slow (Valdez-Taubas and Pelham, 2003), continued pheromone exposure leads to a situation in which Ste2 concentration is highest near the polarity site. G protein subunits are thought to traffic together with the receptor (Suchkov et al., 2010), and using a functional GFP-Ste4 (Gβ) probe, we confirmed that the Gβγ distribution became more polarized at higher pheromone concentrations (Figures 4A and 4B).

Given receptor and G protein polarization, exposure of cells to uniform pheromone would lead to a polarized distribution of free Gβγ and a polarized recruitment of Cdc24. To ask whether this would constrain wandering, we added a new coarse-grained molecular species, RecGEF, to represent the aggregate behavior of the pheromone receptor (Rec), the G protein, and the Far1-Cdc24 complex (GEF) (Figure 4C). RecGEF was delivered on secretory vesicles to the plasma membrane, where it diffused slowly and could bind to extracellular pheromone, becoming RecGEF*, which is an active GEF. RecGEF* was then concentrated into

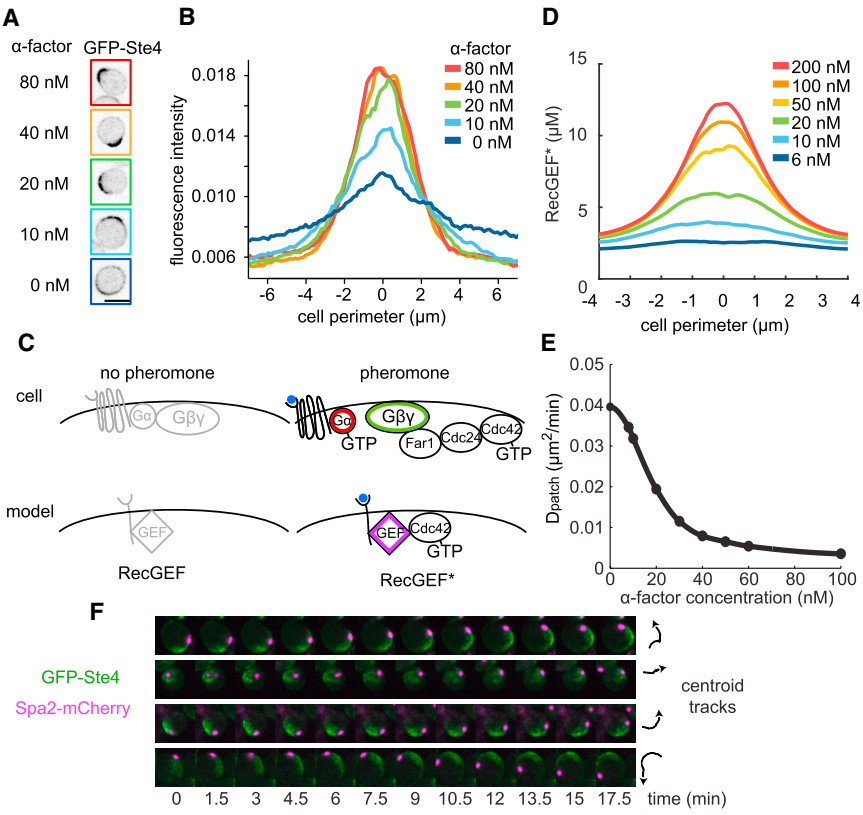

Figure 4. GEF Recruitment Is Polarized, and Polarized GEF Recruitment Would Be Sufficient to Constrain Wandering

(A) Cells (DLY18172) were treated with β-estradiol for 4 hr to induce Ste5-CTM, placed on slabs with the indicated dose of pheromone for 20 min, and then imaged (medial confocal plane).

(B) Quantification of GFP-Ste4 distribution along the cell perimeter (n > 50 cells for each concentration).

(C) The pheromone-sensing machinery in cells (top) was represented by a single RecGEF species in the model (bottom).

(D) RecGEF* distributions from model exposed to different pheromone doses (100 2-hr simulations at each dose).

(E) The effective patch diffusion coefficients from model with RecGEF and exposed to different pheromone doses (100 2-hr simulations at each dose).

(F) Cells (DLY18478) with *cdc24-m1* mutation to uncouple Gβγ from GEF recruitment were treated with β-estradiol for 4 hr, loaded on an 80 nM α-factor slab, and imaged 20 min later. A montage of maximum projection images with Spa2-mCherry centroid tracks is shown on the right.

See also Figure S4 and Movies S4 and S5.

endocytic vesicles, and its activity was terminated upon endocytosis. Exocytosis and endocytosis rates were balanced so that total membrane area and total receptor concentration were constant. This simplified strategy provided a receptor-associated GEF activity whose distribution varied with the pheromone concentration (Figure 4D).

Unlike uniform GEF activity (Figure 3G), the polarized RecGEF* provided a robust constraint on polarity patch wandering in the presence of pheromone (Figure 4E). With enough pheromone, the patch simply wiggled in place: any movement induced by vesicle fusion was rapidly reversed by the Gβγ-recruited GEF (Movie S4). This striking result suggests that trafficking and consequent polarization of the receptor and G protein signaling would be sufficient to constrain polarity patch wandering.

Why Does the Polarized RecGEF* Constrain Patch Wandering when Uniform GEF Does Not?

To better understand how RecGEF* affects polarity patch movement, we generated simulations in which all actin cables (and hence exocytic events) were artificially constrained to occur on a quadrant northeast of the polarity patch (Figure S4A). In the absence of pheromone (no RecGEF*), off-center vesicle delivery of vesicles northeast of the patch diluted polarity factors on that side causing the distribution of GTP-Cdc42 to be asymmetric (Figure S4B). The dilution effect "pushed" the patch centroid away and caused the patch to move consistently southwest (Movie S5). Thus, vesicle delivery acts as a negative feedback on polarity, with a time delay due to the time required to recruit new actin cables to the shifting peak of GTP-Cdc42.

In the presence of pheromone, the speed of patch movement decreased at higher pheromone concentrations (Figure S4C). Moreover, the peak of the RecGEF* distribution lagged behind the polarity patch (Figure S4D). The same vesicles that dilute polarity factors also deliver RecGEF to the cortex. Once pheromone binds to the newly arrived RecGEF, the resulting active RecGEF* raises the GTP-Cdc42 concentration "behind" the moving patch, thereby reducing patch movement. In effect, RecGEF provides a delayed positive feedback that counteracts the dilution-mediated negative feedback from vesicle fusion.

To understand why the RecGEF* is offset behind the Cdc42 patch, consider that pheromone binding is slow (Bajaj et al., 2004; Raths et al., 1988), so there is a time lag between the arrival of a RecGEF at the membrane and its binding to pheromone to generate RecGEF*. During this time lag, the Cdc42 patch moves away from the exocytosis site where the RecGEF was deposited, so the RecGEF* peak is located where the Cdc42 patch was prior to vesicle fusion. In that way, the time lag in pheromone binding is converted into a spatial offset in the direction of patch movement. The spatial offset becomes smaller in high pheromone (Figure S4D), because the patch moves more slowly (Figure S4C).

If RecGEF* were unable to catalyze Cdc42 GTP loading, the patch would continue to move unimpeded, and the spatial offset would be larger (Figures S4E and S4F). Thus, the model predicts that in conditions where the polarized receptor and Gβγ are unable to recruit GEF to constrain wandering (*cdc24-m1* mutants), activated receptors and G proteins should trail the wandering patch. In cells where the polarity patch migrated in a consistent direction, the polarized Gβ crescent could be seen to trail behind the Spa2-marked polarity patch (Figure 4F). Thus, consistent with the model simulations, a spatial offset between the G protein and the polarity peak is detected when constraint of wandering is disabled.

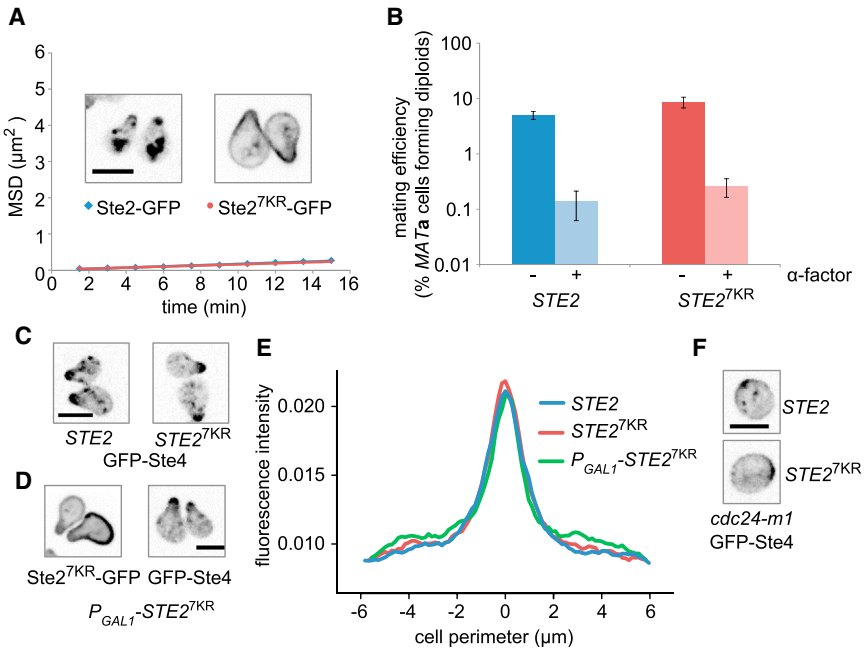

Figure 5. Non-endocytosable Receptor Does Not Affect Constraint of Wandering, Gradient Tracking, or G Protein Polarization

(A) Cells harboring *STE2*^{7KR} (red, DLY15685) or *STE2* (blue, DLY11065) were pretreated with 300 nM α-factor for 1 hr, loaded on an α-factor slab, then imaged. Polarity patch wandering was calculated as MSD from Bem1-GFP centroids (n > 37 cells). Inset: cells expressing Ste2-GFP (DLY15655) or Ste2^{7KR}-GFP (DLY15656) were treated with 300 nM α-factor for 2.5 hr and then imaged (medial confocal plane).

(B) Cells harboring *STE2*^{7KR} (DLY15685) or *STE2* (DLY11740) were assayed for mating efficiency in the presence or absence of excess α-factor to obscure the gradient.

(C) Cells harboring *STE2* (DLY15596) or *STE2*^{7KR} (DLY15717) were pretreated with 300 nM α-factor for 2.5 hr, loaded on α-factor slabs, then imaged (medial confocal plane).

(D) Cells harboring P_{GAL1}-*STE2*^{7KR} were grown in galactose media, switched to dextrose for 1 hr, treated with 300 nM α-factor for 2 hr, loaded on α-factor slabs, and imaged for Ste2^{7KR}-GFP (DLY16078) or GFP-Ste4 (DLY16120) (medial confocal plane).

(E) Cells were treated as in (C) and (D) except that the α-factor treatment was shortened to 1 hr to reduce morphology variations. The graph shows GFP-Ste4 distributions (n > 48 cells).

(F) Cells harboring the *cdc24-m1* mutation and either *STE2* (DLY15719) or *STE2*^{7KR} (DLY15715) were treated as in (C).

Receptor Endocytosis Is Not Necessary to Constrain Wandering

Our findings provide an attractive explanation for why it would be advantageous for yeast cells to polarize their pheromone-sensing machinery during mating: only by polarizing receptors or G proteins can pheromone constrain wandering. If Ste2 polarization is necessary to constrain polarity patch wandering, then reducing polarization by blocking Ste2 endocytosis should impair constraint of wandering. To block receptor endocytosis, we utilized a mutant receptor (designated Ste2^{7KR}) in which the ubiquitination sites and the NPF endocytosis motif are mutated (Chen and Konopka, 1996; Hicke et al., 1998; Terrell et al., 1998). Despite a significantly less polarized distribution of Ste2 (Figure 5A, inset), wandering was still constrained in Ste2^{7KR} cells upon exposure to a high pheromone concentration (Figure 5A). Moreover, Ste2^{7KR} cells exhibited a mating efficiency comparable to that of cells expressing wild-type Ste2 (Figure 5B). Mating efficiency was reduced upon addition of excess pheromone to obscure the spatial gradient (Figure 5B), indicating that Ste2^{7KR} mutants were competent to detect the gradient and bias growth toward mating partners. Thus, endocytosis of Ste2 is not necessary to constrain polarity patch wandering or track pheromone gradients.

Gβγ Can Polarize Independently of Receptor Endocytosis

Previous work suggested that following acute exposure to pheromone, G protein subunits were internalized and then polarized together with the receptor (Suchkov et al., 2010). However, we found that following prolonged exposure to pheromone, GFP-Ste4 (Gβ) became polarized to a similar degree in Ste2^{7KR} and Ste2 (wild-type) cells (Figures 5C and 5E). As Ste2^{7KR} showed some residual polarization (Figure 5A), Ste4 polarization might still be at least partly due to the receptor. To address that possibility, we generated a strain in which Ste2^{7KR} expression was driven by a galactose-inducible promoter. Cells were grown on galactose media, shifted to dextrose to shut off Ste2^{7KR} expression, and arrested with pheromone. In this case, Ste2^{7KR} was not polarized (indeed, in some cells Ste2^{7KR} was *less* concentrated in the shmoo than elsewhere) (Figure 5D). Nevertheless, GFP-Ste4 became polarized to a similar degree even when expression of Ste2^{7KR} was repressed (Figures 5D and 5E). To ask whether Gβγ became polarized through the Cdc24-Far1-Gβγ interactions, we imaged GFP-Ste4 in cells harboring *cdc24-m1* and *STE2*^{7KR}. GFP-Ste4 was still polarized (Figure 5F), suggesting that free Gβγ polarizes independently of the Far1-Cdc24 link. These unexpected findings suggest that Gβγ can be polarized independent of the receptor, raising the possibility that constraint of wandering in strains with Ste2^{7KR} stems from the continuing presence of polarized G protein signaling.

Unpolarized Free Gβγ Does Not Constrain Polarity Patch Wandering

To ask whether Gβγ polarization is required to constrain wandering, we need to examine cells that cannot effectively polarize Gβγ. Although Gβγ was polarized upon treatment of cells expressing Ste5-CTM with high-dose pheromone (Figures 4A and 4B), we found that deletion of Gα (encoded by *GPA1*) prevented

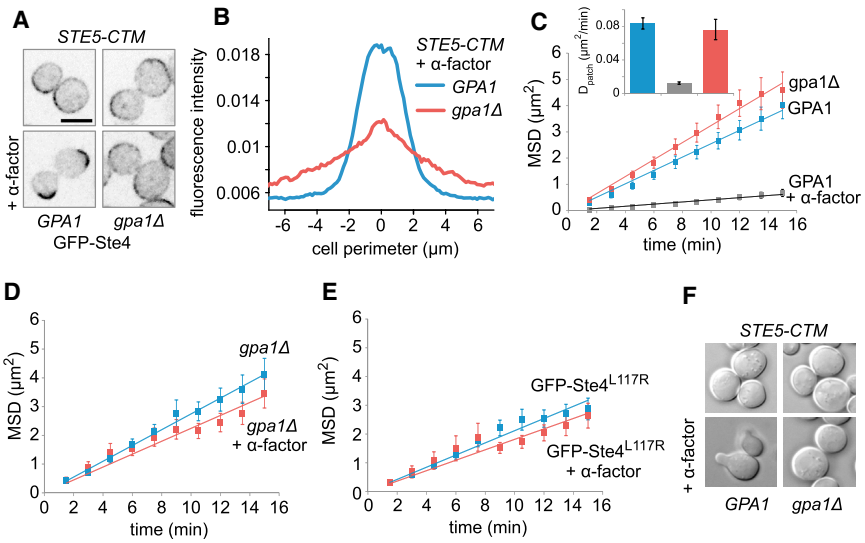

Figure 6. Unpolarized Free Gβγ Cannot Constrain Polarity Patch Wandering

(A) *ste5Δ* P_{GAL1}-*STE5-CTM* cells with or without Gα (*GPA1*, DLY18172;*gpa1Δ*, DLY18559) were treated with β-estradiol for 4 hr, then loaded on a slab with or without 80 nM α-factor for 20 min and imaged (medial confocal plane).

(B) GFP-Ste4 distributions for cells in (A) (n > 42 cells).

(C) Cells were treated as in (A) and imaged. MSD was calculated from Spa2-mCherry centroids (n > 49 cells for each). Inset: effective diffusion coefficient of the polarity patch was calculated from the slope of the MSD lines. Mean ± SEM for nine, six, and five independent biological replicates are shown, respectively.

(D) Cells were treated as in (A) and imaged. MSD was calculated from Spa2-mCherry centroids (n > 49 for each).

(E) Cells with the Gα-binding mutant GFP-Ste4^{L117R} (DLY18195) were analyzed as in (D) (n > 61).

(F) Cells were treated as in (A), but loaded on slabs with or without 300 nM α-factor for 1 hr.

See also Movie S6.

effective Gβγ polarization (Figures 6A and 6B). Thus, at least under these circumstances (we used inducible Ste5-CTM so that *gpa1Δ* cells would be able to grow), Gα is important for Gβγ to polarize. We suspect that Gα is also polarized in wild-type cells responding to pheromone, but we have not yet identified a functional fluorescent reporter for Gα to test that assumption. Although cells lacking Gα had ample free Gβγ distributed over the membrane, they exhibited rampant polarity patch wandering comparable to that in cells lacking any free Gβγ (Figures 6C and 6D; Movie S6). Similar results were obtained in a strain that contained Gα but expressed a mutant version of *STE4* (Gβ) that impaired interaction with Gα (Figure 6E) (Strickfaden and Pryciak, 2008). Consistent with these results, cells lacking Gα remained round and failed to grow a projection (Figure 6F) (Strickfaden and Pryciak, 2008). Thus, the ability of cells to polarize Gβγ correlates with their ability to constrain polarity patch wandering.

DISCUSSION

Why Would Yeast Cells Polarize Their Pheromone-Sensing Machinery?

Eukaryotic cells are thought to employ a spatial gradient sensing mechanism in which cells compare chemoattractant concentrations at different points on the cell surface to assess the direction of the gradient (Jin, 2013). For optimal spatial gradient sensing, cells should localize receptors uniformly over the cell surface (Berg and Purcell, 1977; Endres and Wingreen, 2008). *Dictyostelium discoideum* cells indeed localize their receptors all over the membrane and create an activated G protein distribution that faithfully mirrors the externally applied gradient (Janetopoulos et al., 2001; Wang et al., 1988; Xiao et al., 1997). In contrast, yeast cells polarize their receptors and G proteins (Arkowitz, 2009; Ayscough and Drubin, 1998; Moore et al., 2008). Although this would reduce the accuracy of gradient sensing, we now argue that such polarization may actually be helpful in gradient tracking.

During gradient tracking, the yeast polarity patch wanders around the cortex. This behavior arises from the combination of a positive feedback loop that concentrates polarity factors and stochastic local vesicle fusion, which dilutes those same polarity factors (Dyer et al., 2013; Layton et al., 2011; Savage et al., 2012; Watson et al., 2014) and may also deliver negative regulators (Knaus et al., 2007; Ozbudak et al., 2005). Wandering was reduced as pheromone concentration was increased, and the ability of pheromone to constrain wandering required an intact pathway whereby free Gβγ recruits Cdc24 to the cortex. We found through computational modeling that free Gβγ would need to be polarized in order for pheromone to constrain wandering, and consistent with that prediction, generating free Gβγ all over the membrane failed to constrain wandering. These results suggest that polarization of receptor signaling is important for yeast cells to adjust polarity patch wandering in response to the local pheromone concentration. Together, our findings indicate that polarizing the receptor or G protein could provide an important benefit for gradient tracking, offsetting the cost of reduced gradient perception.

Polarized Pheromone Signaling Is Enforced by Gβγ Localization

We found that Gβγ became polarized, even if receptor recycling was blocked, implying the existence of a previously unsuspected receptor-independent Gβγ polarization pathway. Polarizing either the receptor or Gβγ alone would be sufficient to polarize signaling: even in cells with receptor distributed over the cell, only pheromone near the polarity site would yield release of free Gβγ. These findings could explain why *STE2*^{7KR} mutants were still able to constrain wandering.

Implications for Gradient Tracking

Successful mating requires yeast cells to polarize growth toward a potential mating partner. The first step in polarized growth is polarization of Cdc42 via positive feedback. While critical for

polarization, positive feedback has negative consequences for gradient sensing: it amplifies fluctuations, potentially leading to polarization in the wrong direction, and it stabilizes the polarity site, impairing reorientation and error correction. To counterbalance positive feedback, it was proposed that gradient tracking could be enhanced by a localized negative feedback loop (Meinhardt, 1999). The observed wandering of the polarity site suggests that local negative feedback occurs in yeast, due to actin-mediated vesicle delivery that dilutes (and possibly antagonizes) polarity factors. At the same time, exocytic vesicles carry new receptors to the cell surface. These receptors bind pheromone and promote local activation of Cdc42, thus counteracting the negative effect of vesicle fusion in a pheromone-dependent manner. In effect, the polarization of Ste2 and G$\beta\gamma$ creates a sensitive "nose" that wanders along behind the polarity patch, continually checking the pheromone concentration. In cells exposed to uniform pheromone, the effective diffusion coefficient of the patch decreased with pheromone concentration. Thus, the "nose" restrains patch movement when it perceives more pheromone. Extrapolating from our uniform-pheromone experiments to a spatial gradient of pheromone, these findings suggest a simple model for gradient tracking: when the "nose" detects higher pheromone concentrations, wandering is decreased, directing growth up-gradient.

Exploring the behavior of cells in uniform pheromone allowed us to collect enough data to quantify wandering. However, it is possible that the experience of cells in uniform pheromone differs from that of cells in a pheromone gradient. For example, in a gradient, the pheromone concentration detected by the "nose" could change with time, either rising as the patch wandered up-gradient or falling as the patch wandered down-gradient. If yeast cells possessed a "memory" mechanism such that they could compare the current pheromone level with that sensed in the (recent) past, then one could envisage a number of potent enhancements to the rudimentary gradient-tracking mechanism discussed here.

EXPERIMENTAL PROCEDURES

Yeast Strains

Standard molecular genetic procedures were used for strain construction. Yeast strains, plasmids, and construction details are listed in the Supplemental Experimental Procedures.

Live-Cell Microscopy

Cells were grown overnight at 30°C to mid-log phase in Complete Synthetic Media (CSM, MP Biomedicals) supplemented with 0.67% Yeast Nitrogen Base, 2% dextrose, and 0.01% adenine. Cultures were then diluted to OD_{600} = 0.1 just prior to treatment. For Ste5-CTM experiments, cells were treated with 20 nM β-estradiol (Sigma) for 4 hr, then mounted on a 2% agarose (Denville Scientific) slab with β-estradiol and α-factor (Genway Biotech), and incubated for 20 min at room temperature prior to imaging. Slab edges were sealed with petroleum jelly. For *STE5* experiments, cells were pre-treated with α-factor in culture for 1 hr for MSD experiments or 1–2.5 hr for still images of cells with fully formed mating projections. Cells were imaged as in Dyer et al. (2013) and described in more detail in the Supplemental Experimental Procedures.

MSD Analysis

Polarity patch tracking was performed using Volocity software (Improvision). The 3D centroid of each patch was calculated after thresholding the Spa2-mCherry or Bem1-GFP patch. To account for stage drift, 0.2 μm TetraSpeck beads (Invitrogen, now Thermo Fisher Scientific) were added to the slab, and the centroid of the bead was subtracted from each patch centroid. MSD was calculated for each cell as in Dyer et al. (2013). Data were fit with a linear regression forcing the line of best fit through the origin, and the diffusion coefficient was extracted from the slope.

Distribution Analysis

Using FIJI software, the average intensity of a 3-pixel-wide line drawn with the freehand line tool on the cell perimeter was measured. For the single-cell tracings in Figure 1D, fluorescence values were normalized by subtracting the minimum value and then dividing by the maximum. For the population averages in Figures 4B, 5E, and 6B, the GFP-Ste4 distribution for each cell was fit with a spline using the smooth.spline function in the statistical software R with a smoothing parameter of 0.75. The cells were then aligned by the maximum of their spline function. The raw fluorescence values for each cell were then normalized to an integral of 1. All cells in the sample were then averaged, and if less than 30 cells contributed to a given point along the cell perimeter, then it was not included.

Computational Modeling

Polarity Establishment Module

This module considers the interactions between Cdc42, a Bem1-GEF complex, and a GDI (Figure 2E; Table S1). GDP-Cdc42 (42D) can bind the GDI (G) to make a complex (G42) that can exchange between membrane and cytoplasm (cytoplasmic species are denoted by the subscript "c"). The Bem1-GEF complex (BG) can also exchange between membrane and cytoplasm. BG can bind GTP-Cdc42 (42T) to make a complex (BG42). Both BG and BG42 have GEF activity and can stimulate conversion of 42D to 42T. GAP-stimulated conversion of 24T to 42D is modeled as a first-order process. Rate constants are listed in Table S2 and model equations in the Supplemental Experimental Procedures.

New Feature. We updated our previous version (Dyer et al., 2013) to include species for free (R) and ligated (RG) receptors. R diffuses on the membrane and can bind to external pheromone (α_f) to generate RG. RG is assumed to have GEF activity. Receptor-associated GEF is distinct from Bem1-associated GEF. Because the fraction of the total GEF that is polarized is small (Wedlich-Soldner et al., 2004), we assume that the two pools are independent (i.e., that Bem1 and the receptor are not competing for a limiting pool of GEF). We note that the two pools of GEF in the model are not distinguishable experimentally because they result from recruitment of the same GEF, Cdc24.

The computational domain was taken to be a square grid with periodic boundary conditions. The length of the domain was approximately 8 μm, generating an area equivalent to that of a spherical cell with 5-μm diameter. To integrate the reaction-diffusion equations, we used a numerical method that treats the reaction and diffusion parts of the equations separately. The diffusion terms were updated using a second order backward-time centered-space finite difference algorithm. To integrate the reaction terms, we used the forward Euler method. Because diffusion of proteins in the yeast plasma membrane is slow relative to the biochemical reactions, we performed 100 iterations of the reaction terms between each update of the diffusion terms. The integration timestep for diffusion was 0.05 s. We assumed that protein species in the cytoplasm diffuse rapidly enough that the cytoplasmic compartment can be treated as well mixed.

Vesicle Trafficking Module

To accommodate vesicle traffic, we added a well-mixed internal membrane compartment and allowed vesicle-sized membrane packets to exchange between the internal compartment and the plasma membrane. Vesicle traffic leads to localized delivery of protein cargo to and from the plasma membrane, which several previous models have considered as deterministic or stochastic protein fluxes (Freisinger et al., 2013; Marco et al., 2007; Slaughter et al., 2009). However, such models ignore the effect of the vesicle membrane that conveys the protein cargo, which can lead to artifactual findings and neglects the possibility that local protein concentrations can be diluted by exocytic vesicle fusion (Layton et al., 2011). Recent experimental findings suggest that Cdc42 is present on vesicles, but at lower concentration than at the polarity site (Watson et al., 2014). Moreover, Bem1 and GEF are not thought to be present on vesicles, so exocytosis would locally dilute the key polarity proteins. Our model accounts for the vesicle membrane as well as the cargo proteins,

thereby allowing for dilution effects and providing a mechanism to explain wandering of the polarity patch.

Exocytic and endocytic events were treated as stochastic processes. On the basis of experimental findings summarized in Dyer et al. (2013) and Layton et al. (2011), we estimate that there are approximately 50 exocytic events and 100 endocytic events per min, on average, and that exocytic and endocytic vesicles have diameters of approximately 100 nm and 50 nm, respectively. Vesicle traffic would therefore lead to net growth of the plasma membrane area with time, as occurs during shmooing. However, for modeling convenience we double the rate of endocytosis so that there is no net growth on average. This reflects the assumption that wandering occurs on a faster timescale than growth, so that to a first approximation growth can be neglected.

Exocytosis

The area of an exocytic vesicle corresponds to four grid points at the plasma membrane, and the concentrations of the various species in those grid points are replaced with the concentrations present on the vesicle. We assume that v-SNAREs and pheromone receptors are concentrated 10-fold on vesicles from their level in the well-mixed internal membrane compartment, while Cdc42 is at the same concentration as on the internal compartment. Exocytic vesicles carry GDP-Cdc42 and newly synthesized free receptors, but no Bem1-GEF complexes. After an exocytic event occurs, membrane proteins are redistributed using a radial interpolation centered at the point of fusion, as described in Savage et al. (2012)

New Feature: Location of Exocytosis. In yeast cells, vesicles are delivered by myosin V motors along actin cables to the polarity site (Pruyne et al., 2004). In the model, we assume that exocytic events occur at one of a limited number of locations, which represent the ends of actin cables. In cells, new cables are nucleated by formins (Moseley and Goode, 2006). Cables remain attached for some time, and cells maintain a steady state with approximately 7–15 cables (Yu et al., 2011). In the model, we accommodate these observations by assuming a total of 10 cables, which can attach to the membrane with probability 20 per s and detach from the membrane with probability 1 per min. This means that all 10 cables will be attached most of the time, but their location will be dynamic.

If a cable association event occurs at time t, we use the 2D probability distribution $P_{cable}(i,j)$ to determine where on the membrane the cable becomes attached. Because formins are recruited by GTP-Cdc42 via at least four weak interactions (Chen et al., 2012; Liu et al., 2012), we used a Hill function with Hill coefficient $n_{42} = 4$ to transform the GTP-Cdc42 distribution:

$$P_{\text{cable}}(i,j) = \frac{1}{Z}\frac{[\text{Cdc42}]^{n_{42}}}{\left([\text{Cdc42}]^{n_{42}} + k_{\text{Cdc42}}^{n_{42}}\right)}, \qquad \text{(Equation 3)}$$

where the constant Z is a normalization factor to ensure that the probability distribution $P_{cable}(i,j)$ sums to 1. The saturation parameter k_{Cdc42} was taken to be the half-maximum of the current GTP-Cdc42 concentration. If a vesicle fusion event occurs at time t, we randomly choose one of the attached cable locations as the fusion site.

Endocytosis

The area of an endocytic vesicle corresponds to one grid point at the plasma membrane. In cells, endocytosis is a multistep process (Kaksonen, 2008). First, an endocytic patch forms through assembly of a "coat" at the plasma membrane. Cargo proteins with endocytic motifs interact with adaptor proteins in the patch and become concentrated within the patch. After a variable interval, coat proteins promote actin assembly nucleated by Arp2/3 complexes, causing invagination and scission of the endocytic vesicle, which then fuses with endosomes. In the model, we include a molecular species with characteristics of an exocytic v-SNARE to guide the location and behavior of endocytic patches. The v-SNARE does not react with any polarity proteins and serves as a stand-in for all endocytic cargo. When a grid point is designated as an endocytic patch (see below), we assume that the site becomes a diffusion trap for any endocytic cargo (v-SNARE and ligated receptors). Other membrane proteins diffuse through the patch unhindered. Cargo trapping continues until a designated "fill level" of v-SNARE is reached, or a maximum cutoff time is reached, triggering internalization (Layton et al., 2011). The contents of the patch then become "frozen" for 15 s, representing the time it takes for vesicle internalization and endosome fusion, after which the contents of the vesicle are transferred to the internal membrane compartment (membrane, v-SNARE, Cdc42) or cytoplasm (GDI, Bem1-GEF). Liganded receptors that are internalized are destroyed (corresponding to vacuolar degradation, their fate in cells). To maintain a constant total receptor content, an equal number of unliganded receptors are introduced into the internal membrane compartment. After an internalization event occurs, membrane proteins are redistributed using a radial interpolation (Savage et al., 2012), centered at the point of fission.

New Feature: Location of Endocytosis. In yeast cells, endocytic patches cluster near sites of exocytosis, possibly because patch initiation is responsive to local cargo concentration. If an endocytic patch forms at time t, we use the 2D probability distribution $P_{endo}(i,j)$ to determine where on the membrane the patch forms. Because patches cluster where cargo concentration is high, we used a Hill function to transform the v-SNARE distribution:

$$P_{\text{endo}}(i,j) = \frac{1}{Z}\frac{[\text{vSNARE}]^{n_v}}{\left([\text{cSNARE}]^{n_v} + k_{\text{vSNARE}}^{n_v}\right)}, \qquad \text{(Equation 4)}$$

where Z is a normalization factor to ensure that the probability distribution sums to 1. The saturation parameter k_{vSNARE} was taken to be the half-maximum of the current v-SNARE concentration.

Vesicle Trafficking Module Parameters

The distribution of exocytic and endocytic events in the model depend on the choice of Hill coefficients in P_{cable} and P_{endo} (Figure S5). These coefficients also affect the degree of wandering exhibited by the polarity patch (Figure S6). We selected $n_{42} = 4$ for the reasons discussed above and $n_v = 3$ because this produced an endocytic patch distribution qualitatively consistent with the distribution of endocytic patches in our cells (Figure 1D). Another important parameter in determining the degree of patch wandering produced by the model is the actin cable lifetime: longer lifetimes yield greater persistence in patch movement and hence more wandering (Dyer et al., 2013). We selected a lifetime of 1 min. Although this yielded somewhat less wandering than that observed in cells induced to express Ste5-CTM, with longer cable lifetimes we saw that cables were sometimes left behind the wandering polarity patch, which seemed unphysiological.

SUPPLEMENTAL INFORMATION

Supplemental Information includes Supplemental Experimental Procedures, six figures, two tables, and six movies and can be found with this article online at http://dx.doi.org/10.1016/j.devcel.2015.10.024.

AUTHOR CONTRIBUTIONS

A.W.M., M.M., J.M.D., T.C.E., and D.J.L. designed experiments and analyzed data; A.W.M. and J.M.D. performed experiments; M.M. performed computational modeling simulations; T.R.Z. generated plasmids and yeast strains; and A.W.M. and D.J.L. wrote the paper with contributions from M.M., J.M.D., and T.C.E.

ACKNOWLEDGMENTS

We thank D. Stone (University of Illinois, Chicago), R. Arkowitz (CNRS, University of Nice, France), L. Hicke (University of Texas, Austin), and P. Pryciak (University of Massachusetts, Worcester) for kind gifts of plasmids and strains. We also thank N. Buchler, S. Di Talia, and members of the D.J.L. lab for critical readings of the manuscript. Special thanks to B. Woods for experimental suggestions and D. McClure for help with data analysis. This work was funded by NIH/NIGMS grant GM103870 to D.J.L. and T.C.E.

Received: March 2, 2015
Revised: September 30, 2015
Accepted: October 26, 2015
Published: November 23, 2015

REFERENCES

Arkowitz, R.A. (2009). Chemical gradients and chemotropism in yeast. Cold Spring Harb. Perspect. Biol. *1*, a001958.

Ayscough, K.R., and Drubin, D.G. (1998). A role for the yeast actin cytoskeleton in pheromone receptor clustering and signalling. Curr. Biol. *8*, 927–930.

Bajaj, A., Celić, A., Ding, F.-X., Naider, F., Becker, J.M., and Dumont, M.E. (2004). A fluorescent alpha-factor analogue exhibits multiple steps on binding to its G protein coupled receptor in yeast. Biochemistry *43*, 13564–13578.

Berg, H.C., and Purcell, E.M. (1977). Physics of chemoreception. Biophys. J. *20*, 193–219.

Bi, E., and Park, H.-O.O. (2012). Cell polarization and cytokinesis in budding yeast. Genetics *191*, 347–387.

Blondel, M., Alepuz, P.M., Huang, L.S., Shaham, S., Ammerer, G., and Peter, M. (1999). Nuclear export of Far1p in response to pheromones requires the export receptor Msn5p/Ste21p. Genes Dev. *13*, 2284–2300.

Butty, A.C., Pryciak, P.M., Huang, L.S., Herskowitz, I., and Peter, M. (1998). The role of Far1p in linking the heterotrimeric G protein to polarity establishment proteins during yeast mating. Science *282*, 1511–1516.

Chen, Q., and Konopka, J.B. (1996). Regulation of the G-protein-coupled alpha-factor pheromone receptor by phosphorylation. Mol. Cell. Biol. *16*, 247–257.

Chen, H., Kuo, C.-C.C., Kang, H., Howell, A.S., Zyla, T.R., Jin, M., and Lew, D.J. (2012). Cdc42p regulation of the yeast formin Bni1p mediated by the effector Gic2p. Mol. Biol. Cell *23*, 3814–3826.

Condeelis, J., Singer, R.H., and Segall, J.E. (2005). The great escape: when cancer cells hijack the genes for chemotaxis and motility. Annu. Rev. Cell Dev. Biol. *21*, 695–718.

Dyer, J.M., Savage, N.S., Jin, M., Zyla, T.R., Elston, T.C., and Lew, D.J. (2013). Tracking shallow chemical gradients by actin-driven wandering of the polarization site. Curr. Biol. *23*, 32–41.

Endres, R.G., and Wingreen, N.S. (2008). Accuracy of direct gradient sensing by single cells. Proc. Natl. Acad. Sci. USA *105*, 15749–15754.

Freisinger, T., Klünder, B., Johnson, J., Müller, N., Pichler, G., Beck, G., Costanzo, M., Boone, C., Cerione, R.A., Frey, E., and Wedlich-Söldner, R. (2013). Establishment of a robust single axis of cell polarity by coupling multiple positive feedback loops. Nat. Commun. *4*, 1807.

Fujiwara, T., Tanaka, K., Mino, A., Kikyo, M., Takahashi, K., Shimizu, K., and Takai, Y. (1998). Rho1p-Bni1p-Spa2p interactions: implication in localization of Bni1p at the bud site and regulation of the actin cytoskeleton in Saccharomyces cerevisiae. Mol. Biol. Cell *9*, 1221–1233.

Goryachev, A.B., and Pokhilko, A.V. (2008). Dynamics of Cdc42 network embodies a Turing-type mechanism of yeast cell polarity. FEBS Lett. *582*, 1437–1443.

Hao, N., Nayak, S., Behar, M., Shanks, R.H., Nagiec, M.J., Errede, B., Hasty, J., Elston, T.C., and Dohlman, H.G. (2008). Regulation of cell signaling dynamics by the protein kinase-scaffold Ste5. Mol. Cell *30*, 649–656.

Harold, F.M. (1990). To shape a cell: an inquiry into the causes of morphogenesis of microorganisms. Microbiol. Rev. *54*, 381–431.

Hicke, L., and Riezman, H. (1996). Ubiquitination of a yeast plasma membrane receptor signals its ligand-stimulated endocytosis. Cell *84*, 277–287.

Hicke, L., Zanolari, B., and Riezman, H. (1998). Cytoplasmic tail phosphorylation of the alpha-factor receptor is required for its ubiquitination and internalization. J. Cell Biol. *141*, 349–358.

Insall, R. (2013). The interaction between pseudopods and extracellular signalling during chemotaxis and directed migration. Curr. Opin. Cell Biol. *25*, 526–531.

Jackson, C.L., Konopka, J.B., and Hartwell, L.H. (1991). S. cerevisiae alpha pheromone receptors activate a novel signal transduction pathway for mating partner discrimination. Cell *67*, 389–402.

Janetopoulos, C., Jin, T., and Devreotes, P. (2001). Receptor-mediated activation of heterotrimeric G-proteins in living cells. Science *291*, 2408–2411.

Jenness, D.D., and Spatrick, P. (1986). Down regulation of the alpha-factor pheromone receptor in S. cerevisiae. Cell *46*, 345–353.

Jenness, D.D., Burkholder, A.C., and Hartwell, L.H. (1986). Binding of alpha-factor pheromone to Saccharomyces cerevisiae a cells: dissociation constant and number of binding sites. Mol. Cell. Biol. *6*, 318–320.

Jin, T. (2013). Gradient sensing during chemotaxis. Curr. Opin. Cell Biol. *25*, 532–537.

Kaksonen, M. (2008). Taking apart the endocytic machinery. J. Cell Biol. *180*, 1059–1060.

Kaksonen, M., Sun, Y., and Drubin, D.G. (2003). A pathway for association of receptors, adaptors, and actin during endocytic internalization. Cell *115*, 475–487.

Knaus, M., Pelli-Gulli, M.P., van Drogen, F., Springer, S., Jaquenoud, M., and Peter, M. (2007). Phosphorylation of Bem2p and Bem3p may contribute to local activation of Cdc42p at bud emergence. EMBO J. *26*, 4501–4513.

Kozubowski, L., Saito, K., Johnson, J.M., Howell, A.S., Zyla, T.R., and Lew, D.J. (2008). Symmetry-breaking polarization driven by a Cdc42p GEF-PAK complex. Curr. Biol. *18*, 1719–1726.

Lawson, M.J., Drawert, B., Khammash, M., Petzold, L., and Yi, T.-M.M. (2013). Spatial stochastic dynamics enable robust cell polarization. PLoS Comput. Biol. *9*, e1003139.

Layton, A.T., Savage, N.S., Howell, A.S., Carroll, S.Y., Drubin, D.G., and Lew, D.J. (2011). Modeling vesicle traffic reveals unexpected consequences for Cdc42p-mediated polarity establishment. Curr. Biol. *21*, 184–194.

Liu, W., Santiago-Tirado, F.H., and Bretscher, A. (2012). Yeast formin Bni1p has multiple localization regions that function in polarized growth and spindle orientation. Mol. Biol. Cell *23*, 412–422.

Madden, K., and Snyder, M. (1992). Specification of sites for polarized growth in Saccharomyces cerevisiae and the influence of external factors on site selection. Mol. Biol. Cell *3*, 1025–1035.

Marco, E., Wedlich-Soldner, R., Li, R., Altschuler, S.J., and Wu, L.F. (2007). Endocytosis optimizes the dynamic localization of membrane proteins that regulate cortical polarity. Cell *129*, 411–422.

McCudden, C.R., Hains, M.D., Kimple, R.J., Siderovski, D.P., and Willard, F.S. (2005). G-protein signaling: back to the future. Cell. Mol. Life Sci. *62*, 551–577.

Meinhardt, H. (1999). Orientation of chemotactic cells and growth cones: models and mechanisms. J. Cell. Sci. *112*, 2867–2874.

Moore, T.I., Chou, C.-S., Nie, Q., Jeon, N.L., and Yi, T.-M. (2008). Robust spatial sensing of mating pheromone gradients by yeast cells. PLoS ONE *3*, e3865.

Moseley, J.B., and Goode, B.L. (2006). The yeast actin cytoskeleton: from cellular function to biochemical mechanism. Microbiol. Mol. Biol. Rev. *70*, 605–645.

Mulholland, J., Wesp, A., Riezman, H., and Botstein, D. (1997). Yeast actin cytoskeleton mutants accumulate a new class of Golgi-derived secretary vesicle. Mol. Biol. Cell *8*, 1481–1499.

Nern, A., and Arkowitz, R.A. (1998). A GTP-exchange factor required for cell orientation. Nature *391*, 195–198.

Nern, A., and Arkowitz, R.A. (1999). A Cdc24p-Far1p-Gbetagamma protein complex required for yeast orientation during mating. J. Cell Biol. *144*, 1187–1202.

Nern, A., and Arkowitz, R.A. (2000). G proteins mediate changes in cell shape by stabilizing the axis of polarity. Mol. Cell *5*, 853–864.

Ozbudak, E.M., Becskei, A., and van Oudenaarden, A. (2005). A system of counteracting feedback loops regulates Cdc42p activity during spontaneous cell polarization. Dev. Cell *9*, 565–571.

Paliwal, S., Iglesias, P.A., Campbell, K., Hilioti, Z., Groisman, A., and Levchenko, A. (2007). MAPK-mediated bimodal gene expression and adaptive gradient sensing in yeast. Nature *446*, 46–51.

Pruyne, D., Legesse-Miller, A., Gao, L., Dong, Y., and Bretscher, A. (2004). Mechanisms of polarized growth and organelle segregation in yeast. Annu. Rev. Cell Dev. Biol. *20*, 559–591.

Pryciak, P.M., and Huntress, F.A. (1998). Membrane recruitment of the kinase cascade scaffold protein Ste5 by the Gbetagamma complex underlies activation of the yeast pheromone response pathway. Genes Dev. *12*, 2684–2697.

Rappel, W.J., and Loomis, W.F. (2009). Eukaryotic chemotaxis. Wiley Interdiscip. Rev. Syst. Biol. Med. *1*, 141–149.

Raths, S.K., Naider, F., and Becker, J.M. (1988). Peptide analogues compete with the binding of alpha-factor to its receptor in Saccharomyces cerevisiae. J. Biol. Chem. *263*, 17333–17341.

Raz, E., and Reichman-Fried, M. (2006). Attraction rules: germ cell migration in zebrafish. Curr. Opin. Genet. Dev. *16*, 355–359.

Savage, N.S., Layton, A.T., and Lew, D.J. (2012). Mechanistic mathematical model of polarity in yeast. Mol. Biol. Cell *23*, 1998–2013.

Schandel, K.A., and Jenness, D.D. (1994). Direct evidence for ligand-induced internalization of the yeast alpha-factor pheromone receptor. Mol. Cell. Biol. *14*, 7245–7255.

Schnorrer, F., and Dickson, B.J. (2004). Axon guidance: morphogens show the way. Curr. Biol. *14*, R19–R21.

Segall, J.E. (1993). Polarization of yeast cells in spatial gradients of alpha mating factor. Proc. Natl. Acad. Sci. USA *90*, 8332–8336.

Shimada, Y., Gulli, M.P., and Peter, M. (2000). Nuclear sequestration of the exchange factor Cdc24 by Far1 regulates cell polarity during yeast mating. Nat. Cell Biol. *2*, 117–124.

Slaughter, B.D., Das, A., Schwartz, J.W., Rubinstein, B., and Li, R. (2009). Dual modes of cdc42 recycling fine-tune polarized morphogenesis. Dev. Cell *17*, 823–835.

Smith, S.E., Rubinstein, B., Mendes Pinto, I., Slaughter, B.D., Unruh, J.R., and Li, R. (2013). Independence of symmetry breaking on Bem1-mediated autocatalytic activation of Cdc42. J. Cell Biol. *202*, 1091–1106.

Sourjik, V., and Wingreen, N.S. (2012). Responding to chemical gradients: bacterial chemotaxis. Curr. Opin. Cell Biol. *24*, 262–268.

Strickfaden, S.C., and Pryciak, P.M. (2008). Distinct roles for two Galpha-Gbeta interfaces in cell polarity control by a yeast heterotrimeric G protein. Mol. Biol. Cell *19*, 181–197.

Suchkov, D.V., DeFlorio, R., Draper, E., Ismael, A., Sukumar, M., Arkowitz, R., and Stone, D.E. (2010). Polarization of the yeast pheromone receptor requires its internalization but not actin-dependent secretion. Mol. Biol. Cell *21*, 1737–1752.

Swaney, K.F., Huang, C.-H.H., and Devreotes, P.N. (2010). Eukaryotic chemotaxis: a network of signaling pathways controls motility, directional sensing, and polarity. Annu. Rev. Biophys. *39*, 265–289.

Terrell, J., Shih, S., Dunn, R., and Hicke, L. (1998). A function for monoubiquitination in the internalization of a G protein-coupled receptor. Mol. Cell *1*, 193–202.

Valdez-Taubas, J., and Pelham, H.R.B. (2003). Slow diffusion of proteins in the yeast plasma membrane allows polarity to be maintained by endocytic cycling. Curr. Biol. *13*, 1636–1640.

Valtz, N., Peter, M., and Herskowitz, I. (1995). FAR1 is required for oriented polarization of yeast cells in response to mating pheromones. J. Cell Biol. *131*, 863–873.

von Philipsborn, A., and Bastmeyer, M. (2007). Mechanisms of gradient detection: a comparison of axon pathfinding with eukaryotic cell migration. Int. Rev. Cytol. *263*, 1–62.

Walch-Solimena, C., Collins, R.N., and Novick, P.J. (1997). Sec2p mediates nucleotide exchange on Sec4p and is involved in polarized delivery of post-Golgi vesicles. J. Cell Biol. *137*, 1495–1509.

Wang, M., Van Haastert, P.J., Devreotes, P.N., and Schaap, P. (1988). Localization of chemoattractant receptors on Dictyostelium discoideum cells during aggregation and down-regulation. Dev. Biol. *128*, 72–77.

Watson, L.J., Rossi, G., and Brennwald, P. (2014). Quantitative analysis of membrane trafficking in regulation of Cdc42 polarity. Traffic *15*, 1330–1343.

Wedlich-Soldner, R., Altschuler, S., Wu, L., and Li, R. (2003). Spontaneous cell polarization through actomyosin-based delivery of the Cdc42 GTPase. Science *299*, 1231–1235.

Wedlich-Soldner, R., Wai, S.C., Schmidt, T., and Li, R. (2004). Robust cell polarity is a dynamic state established by coupling transport and GTPase signaling. J. Cell Biol. *166*, 889–900.

Xiao, Z., Zhang, N., Murphy, D.B., and Devreotes, P.N. (1997). Dynamic distribution of chemoattractant receptors in living cells during chemotaxis and persistent stimulation. J. Cell Biol. *139*, 365–374.

Yu, J.H., Crevenna, A.H., Bettenbühl, M., Freisinger, T., and Wedlich-Söldner, R. (2011). Cortical actin dynamics driven by formins and myosin V. J. Cell Sci. *124*, 1533–1541.